Viscid/Inviscid Interaction Analysis of Separated Trailing-Edge Flows

Veer N. Vatsa* and Joseph M. Verdon†
United Technologies Research Center, East Hartford, Connecticut

An analytical procedure based on finite Reynolds number, viscid/inviscid interaction theory is presented for predicting high Reynolds number flow past an airfoil trailing edge. This effort stems from the need to provide efficient prediction methods for local strong interaction regions and, in particular, local flow separations. Attention is focused on subsonic laminar flow past a thin-airfoil trailing edge where local separation is induced by airfoil thickness or loading. Solutions are determined using interacting boundary-layer theory in which the outer inviscid and inner viscous flows are determined simultaneously and matched through a global semi-inverse iteration procedure until a converged result for the complete flowfield is obtained. Detailed results for attached and separated laminar trailing-edge flows are presented including streamline patterns for thick and loaded trailing edges.

Introduction

FOR flows of practical interest in either external or internal aerodynamics the Reynolds number is usually sufficiently high so that the flow over an airfoil or blade can be divided into two regions: an "inner" dissipative region consisting of the boundary layer and wake, and an "outer" inviscid region. The principal interaction between the viscid and inviscid regions arises from the displacement thickness effect which leads to a thickened semi-infinite equivalent body with corresponding changes in surface pressures. If the interaction is "weak," i.e., the viscous effect on the pressure is small, the complete flow problem can be solved sequentially. This traditional approach for calculating the interaction between the viscous and inviscid parts of the flow is based on a direct hierarchy between the viscous and inviscid regions which is applicable as long as the disturbances to the inviscid flow due to the viscous displacement effect are small.

However, the flow over an airfoil involves both a weak overall interaction arising from standard displacement effects, and also from wake curvature effects, and local strong-displacement interactions. In particular, at an airfoil trailing edge strong interactions arise from the abrupt change in the slip condition that the boundary layer experiences at the termination of the airfoil surface as well as from the separation of the viscous layer from the airfoil surface. These features lead to singularities in a classical boundary-layer solution and a subsequent breakdown of a weak-interaction solution procedure. In addition, viscous displacements in the strong-interaction region cause substantial changes in the local inviscid pressure field. The concept of an inner viscous region and an outer inviscid region still holds, but the classical hierarchical structure of the flow no longer applies. Thus in a local strong-interaction region the hierarchy changes from direct (i.e., pressure determined by the inviscid flow) to interactive (i.e., pressure determined by a mutual interaction betwen the inviscid flow and the viscous layer) and this change must be accommodated in the development of a local solution.

The approach taken here employs an interacting boundary-layer model, in which the flow in the outer inviscid region is potential and the viscous flow is governed by Prandtl's boundary-layer equations, to calculate the flow in the trailing-edge and near-wake regions of an airfoil. The primary purpose of the present study is to provide an efficient prediction scheme for finite Reynolds number (Re), separated trailing-edge flows. Thus consideration has been restricted to laminar flows past thin-airfoil trailing edges to keep the overall analysis and inviscid flow representation as simple as possible. The present effort is a continuation of the work reported in Ref. 1 in which laminar flow past the trailing edge of a thin cambered airfoil was considered and solutions were presented for attached flows and flows with small reverse-flow regions. Here the emphasis is on determining the effects of airfoil thickness and loading on trailing-edge flow behavior and, in particular, on trailing-edge separation phenomena.

One-Sided Separation

If separation occurs at the trailing edge of a lightly loaded airfoil, it is reasonable to anticipate that a local region of reverse flow would appear adjacent to the suction surface of the airfoil. However, the mathematical resolution of such a separated flow pattern has proved to be a difficult task (c.f., Refs. 2-4). According to Smith[5] the central question arises because of the Rott-Hakkinen condition.[2] This condition states that if the flow at the trailing edge is forward on one surface of the airfoil then it must also be forward on the other surface, otherwise no solution to the shear-layer equations can be found. Therefore, it has been argued that once a one-sided separation occurs it must be accompanied by a catastrophic stall since the Rott-Hakkinen condition would be violated.

In recent studies, Smith[5,6] presented very convincing numerical evidence, based on the asymptotic triple-deck ($Re \to \infty$) model, which indicates that one-sided closed separation bubbles at a loaded trailing edge can be predicted without violating the Rott-Hakkinen condition. He achieved this by demonstrating that if separation occurs on one side of an airfoil a region of very small but finite extent exists just upstream of the trailing edge in which the pressure drops. This produces a sizable favorable pressure gradient which forces the flow to reattach on the airfoil surface just before it merges into the wake. Although it is not practical to resolve such a small-scale flow structure using a finite Reynolds number interacting-boundary-layer analysis, the separated flow results presented in this paper, along with the recent results of Veldman[7,8] and those of the present authors[1] appear to confirm Smith's contention that one-sided separation regions can be predicted within the framework of a viscous/inviscid interaction theory.

Received Oct. 4, 1983; presented as Paper 84-0266 at the AIAA 22nd Aerospace Sciences Meeting, Reno, Nev., Jan. 9-12, 1984; revision received April 13, 1984.

*Research Engineer, Computational Fluid Mechanics; currently with: NASA Langley Research Center, Hampton, Va. Member AIAA.

†Principal Scientist, Computational Fluid Mechanics. Associate Fellow AIAA.

Problem Description and Formulation

In the following discussion flow variables and spatial coordinates have been made dimensionless. Lengths have been scaled with respect to the length of the airfoil (L^*), density, velocity, and viscosity with respect to their freestream values (ρ^*_∞, U^*_∞, and μ^*_∞, respectively), pressure with respect to twice the freestream dynamic pressure ($\rho^*_\infty U^{*2}_\infty$), and temperature with respect to the square of the freestream speed divided by the specific heat at constant pressure (U^{*2}_∞/c^*_p). Here the asterisk denotes a dimensional quantity and the subscript ∞ refers to the flow conditions at infinity.

We consider high Reynolds number ($Re=\rho^*_\infty U^*_\infty L^*/\mu^*_\infty$), adiabatic, laminar flow with negligible body forces of a perfect gas with constant specific heats, linear viscosity law, and unit Prandtl number past the trailing edge of an airfoil (Fig. 1). The flow is two-dimensional (in the x,y plane) and subsonic with freestream velocity U_∞ in the positive x direction. The airfoil is thin, slightly cambered, and situated at small angle of attack relative to the freestream direction. It is located mainly along the interval $[0,1]$ of the x axis. Viscous effects are concentrated in relatively thin layers adjacent to the airfoil surfaces which merge into a thin wake behind the airfoil. The position of the upper and lower surface of the airfoil and wake displacement body are defined by

$$\begin{aligned} y_\pm(x) &= h_\pm(x)\pm\delta_\pm(x), \qquad x\in[0,1] \\ &= h_W(x)\pm\delta_\pm(x), \qquad x>1 \end{aligned} \tag{1}$$

where h_+ and h_- define the upper and lower surfaces of the airfoil, h_W the location of the reference wake streamline, and δ_+ and δ_- the upper- and lower-surface viscous displacement thicknesses (Fig. 1). Note that in Fig. 1 the symbols $\mathcal{S}$, $\mathcal{D}$, and $\mathcal{W}$ refer to the airfoil surface, the displacement surface, and the reference wake streamline, respectively. The latter is an arbitrary curve that emanates from the trailing edge of the airfoil and lies within the actual viscous wake. Under the stated assumptions concerning airfoil shape and orientation and the flow Reynolds number the projection of the airfoil and wake displacement body on the y axis will be small [i.e., of $\mathcal{O}(\epsilon)\ll 1$].

Solutions will be determined for the flow in the trailing-edge region of the airfoil using finite Reynolds number, viscous/inviscid interaction concepts. If the outer inviscid flow is assumed to be isentropic and irrotational, then a velocity potential $\Phi=U_\infty x+\phi$ exists where the first-order (in ϵ) or disturbance potential can be determined by the methods of linearized potential flow theory. The flow in the inner or viscous region is assumed to be governed by Prandtl's boundary-layer equations which, to within the order of approximation considered here, can be solved in terms of coordinates parallel and normal to the freestream direction. In the present analysis viscous displacement effects at the trailing edge are regarded as strong, while wake curvature effects are regarded as weak. This treatment is in accordance with the triple-deck scaling requirements for laminar flow at asymptotically large Reynolds number.[9] Thus, iterative solutions of the inviscid and viscous equations will be repeatedly determined to obtain a converged solution that accounts for strong displacement interactions and the resulting inviscid solution will then be corrected to account for wake curvature interactions.

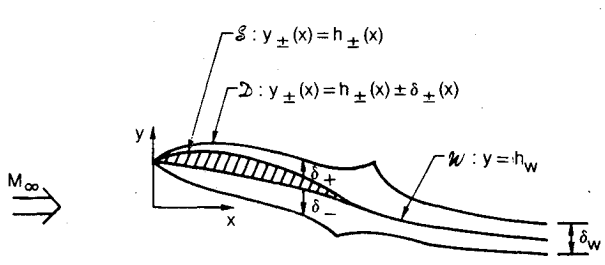

Fig. 1 High Reynolds number flow around a thin airfoil.

The Inviscid Region

The disturbance potential is governed by the linear equation

$$(1-M^2_\infty)\phi_{xx}+\phi_{yy}=0 \tag{2}$$

where M is the Mach number. In addition, the pressure P can be determined from Bernoulli's equation, i.e.,

$$P=P_\infty+p=(\gamma M^2_\infty)^{-1}-\phi_x \tag{3}$$

where $P_\infty=(\gamma M^2_\infty)^{-1}$ is the freestream pressure, p the first order pressure, and γ the specific heat ratio of the fluid. The inviscid flow is determined as a solution of Eq. (2) which is subject to a flow tangency condition at the airfoil displacement surface, jump conditions on normal velocity and pressure across the wake, and the condition of uniform flow in the far field. Since first-order airfoil-surface and wake boundary conditions can be referred to the x axis, it follows that

$$\phi_{y|_{y=0^\pm}}=[h_\pm(x)\pm\delta_\pm(x)]' \quad \text{for} \quad x\in[0,1] \tag{4}$$

$$[\![\phi_y]\!]=\delta'_W(x) \text{ and } [\![p]\!]=\kappa(x)[\delta_W(x)+\theta_W(x)] \quad \text{for } x>1,\ y=0 \tag{5}$$

and

$$\nabla\phi\to 0 \quad \text{as} \quad |x|\to\infty \tag{6}$$

Here the prime denotes differentiation, $[\![\ ]\!]$ denotes the difference (upper minus lower) in a quantity across the wake, δ_W and θ_W are the displacement and momentum thicknesses of the complete wake, respectively, and κ the curvature (positive-concave upwards) of the reference wake streamline. A complication arises in that the location, and, hence, the curvature, of the reference wake streamline is unknown a priori; however, to within lowest order in $\epsilon\sim Re^{-1/2}$ the wake can be represented by an arbitrary curve which emanates from the trailing edge of the airfoil and lies within the actual viscous wake.

Symmetric and Antisymmetric Flows

It is convenient to write the solution to the foregoing problem as the sum of two terms; a symmetric term ϕ^S giving the flow due to thickness effects, and an antisymmetric term ϕ^A giving the flow due to loading effects. Both ϕ^A and ϕ^S must satisfy the differential equation, Eq. (2), and the far-field condition, Eq. (6). In addition, the symmetric component of the potential must satisfy the following condition:

$$\phi^S_y|_{y=0^\pm}=\pm D'_T(x), \qquad x>0 \tag{7}$$

where $D_T=(y_+-y_-)/2$ is one-half the displacement body thickness. Note that the symmetric solution does not produce a pressure difference across the airfoil or its wake. The antisymmetric component of the potential must satisfy the following requirements:

$$\phi^A_y|_{y=0^\pm}=D'_C(x), \qquad x\in[0,1] \tag{8}$$

and

$$[\![\phi_y]\!]=0 \text{ and } [\![p^A]\!]=\kappa(\delta_W+\theta_W), \qquad x>1,\ y=0 \tag{9}$$

where $y=D_c=(y_++y_-)/2$ defines the location of the displacement-body camber line. Clearly, the sum $\phi=\phi^S+\phi^A$ is a solution of the original inviscid boundary-value problem.

A further decomposition of the disturbance velocity potential will be used herein to distinguish between displacement

and wake curvature effects on the outer inviscid flow. Thus, we set $\phi^A = \phi^A_D + \phi^A_{WC}$ where the antisymmetric potential ϕ^A_D due to airfoil geometry and viscous diplacement effects must satisfy condition (8) and the first part of Eq. (9), but it does not contribute to the pressure jump across the wake, while the potential due to wake curvature effects ϕ^A_{WC} must satisfy both conditions in Eq. (9), but it does not contribute to the normal velocity at the airfoil surface.

Inviscid Pressure Distributions

Solutions to the foregoing boundary-value problems can be conveniently determined using complex variable theory, and, in particular, Cauchy's integral formula.[10] It follows that the symmetric component of the pressure acting on the airfoil and wake can be determined in terms of $D_T(x)$ by evaluation of a Cauchy principal-value integral, i.e.,

$$p^S(x,0^\pm) = -\frac{1}{\pi(1-M_\infty^2)^{1/2}} \oint_0^\infty \frac{D_T'(\zeta)}{x-\zeta} d\zeta \tag{10}$$

The antisymmetric component of the pressure, $p^A(x,0^\pm) = \pm [\![p^A(x)]\!]/2$, acting on the airfoil surface is determined as the solution of the integral equation

$$D_C'(x) = \frac{(1-M_\infty^2)^{1/2}}{2\pi}\left[\oint_0^\infty \frac{[\![p^A(\zeta)]\!]}{x-\zeta} d\zeta + \oint_1^\infty \frac{\kappa(\zeta)[\delta_W(\zeta)+\theta_W(\zeta)}{x-\zeta} d\zeta\right] \tag{11}$$

Both displacement and wake curvature effects contribute to this pressure jump. To determine the jump due to displacement effects alone $[\![p^A_D]\!]$, the second term on the right-hand side of Eq. (11) is set equal to zero. Analytical techniques[10] can be used to invert the resulting singular integral equation and provide the following direct solution for the pressure jump due to displacement effects alone:

$$[\![p^A_D]\!] = \frac{-2}{\pi(1-M_\infty^2)^{1/2}}\left(\frac{1-x}{x}\right)^{1/2} \oint_0^1 \frac{D_C'(\zeta)}{x-\zeta}\left(\frac{\zeta}{1-\zeta}\right)^{1/2} d\zeta \tag{12}$$

The pressure jump across the airfoil due to wake curvature is then determined as a solution of the integral equation

$$\oint_0^1 \frac{[\![p^A_{WC}(\zeta)]\!]}{x-\zeta} d\zeta = -\int_1^\infty \frac{\kappa(\zeta)[\delta_W(\zeta)+\theta_W(\zeta)]}{x-\zeta} d\zeta \tag{13}$$

Here, the wake curvature is taken to be the curvature of the inviscid wake camberline as determined by the strong-displacement interaction inviscid solution, i.e.,

$$\kappa(x) = D_c''(x) = \frac{(1-M_\infty^2)^{1/2}}{2\pi}\frac{d}{dx}\int_0^1 \frac{[\![p^A_D(\zeta)]\!]}{x-\zeta} d\zeta, \qquad x>1 \tag{14}$$

Finally, the pressure acting on the airfoil and reference wake streamline is given by

$$p(x,0^\pm) = p^S(x,0) \pm [\![p^A]\!]/2, \qquad x>0 \tag{15}$$

The Viscous Layer

For thin airfoils operating at high Reynolds number, the viscous layer equations (i.e., Prandtl's boundary-layer equations) can be written in terms of coordinates parallel (x) and normal (y) to the freestream direction. After first introducing Prandtl's transformation; i.e.,

$$\tilde{y}_\pm = \pm Re^{1/2}(y-h_\pm)$$
$$\tilde{v}_\pm = \pm Re^{1/2}(v-uh'_\pm) \tag{16}$$

where $h_+ = h_- = h_W$ for $x>1$, u and v are the velocity components in the x and y directions, and the scaled normal coordinate $\tilde{y}$ and normal velocity component $\tilde{v}$ are positive along the outward normal to the x axis, the viscous equations are recast in terms of Levy Lees variables to facilitate their numerical resolution. Thus, with new independent (ξ and η) and dependent (F and V) variables defined by

$$\xi = \xi_I + \int_{x_I}^x \rho_e \mu_e u_e dx, \qquad \eta = \frac{u_e}{\sqrt{2\xi}}\int_0^{\tilde{y}} \rho d\tilde{y} \tag{17}$$

and

$$F = \frac{u}{u_e}, \qquad V = 2\xi\left[F\frac{\partial\eta}{\partial x} + \rho\tilde{v}\sqrt{Re}\,(2\xi)^{-1/2}\right]\Big/\frac{d\xi}{dx} \tag{18}$$

the viscous equations assume the form

$$2\xi\frac{\partial F}{\partial\xi} + \frac{\partial V}{\partial\eta} + F = 0 \tag{19}$$

$$2\xi F\frac{\partial F}{\partial\xi} + V\frac{\partial F}{\partial\eta} + \beta(F^2-1) - \frac{\partial}{\partial\eta}\left(\frac{\partial F}{\partial\eta}\right) = 0 \tag{20}$$

where

$$\beta = \frac{2\xi}{M_e}\frac{dM_e}{d\xi} \tag{21}$$

Here the subscript e refers to the edge of the viscous layer and ρ and μ are the fluid density and viscosity, respectively. Fluid properties at the edge of the viscous layer (i.e., inviscid properties at the displacement surface, $\mathfrak{D}$) are determined from Bernoulli's equation.

The boundary conditions on F and V are as follows

$$F \to 1 \quad \text{for} \quad \eta \to \infty \tag{22}$$

$$F = V = 0 \quad \text{for} \quad \xi \le \xi_{TE}, \qquad \eta = 0 \tag{23}$$

$$V = 0 \quad \text{for} \quad \xi > \xi_{TE}, \qquad \eta = 0 \tag{24}$$

Condition (24) follows from the requirement that the velocity component normal to the reference wake streamline must be zero. For convenience the plus and minus subscripts have been omitted from Eqs. (17-24). To determine the effect of the viscous layer on the outer flow, the displacement and momentum thickness must be evaluated from the upper and lower viscous solutions. It follows from the standard definitions of the displacement thickness δ and the momentum thickness θ, that

$$\rho_e u_e \delta\left(\frac{Re}{2\xi}\right)^{1/2} = \int_0^\infty \left[1 - F + \frac{(\gamma-1)}{2}M_e^2(1-F^2)\right] d\eta \tag{25}$$

and

$$\rho_e u_e \theta\left(\frac{Re}{2\xi}\right)^{1/2} = \int_0^\infty (1-F)F d\eta \tag{26}$$

The displacement and momentum thickness of the complete wake are then given by

$$\delta_W = \delta_+ + \delta_- \quad \text{and} \quad \theta_W = \theta_+ + \theta_- \tag{27}$$

Solution Procedures

The complete flowfield is determined by matching the solutions to the inviscid and viscous equations. In the present analysis simultaneous solutions of the inviscid and viscous equations are determined to account for strong displacement interactions and the resulting inviscid solution is then corrected to account for wake curvature interactions. It has been found that a semi-inverse iteration procedure provides a relatively efficient method for determining the flow in strong viscous/inviscid interaction regions. In this approach the inviscid and viscous equations are solved for a prescribed nth displacement thickness distribution $\delta^n(x)$ to determine the $(n+1)$th inviscid pressure distribution $p_{\text{inv}}^{n+1}(x)$ at the displacement surface from the inviscid solution and the $(n+1)$th viscous pressure distribution, $p_{\text{visc}}^{n+1}(x)$ from the viscous layer solution. The $(n+1)$th estimate for the displacement thickness is then obtained by using the global iteration formula developed by Carter[11]; i.e.,

$$\delta^{n+1}(x)=\delta^n(x)\{1+\omega[p_{\text{inv}}^{n+1}(x)-p_{\text{visc}}^{n+1}(x)]\} \tag{28}$$

where ω is the relaxation parameter. Equation (28) is applied to update the calculated displacement thickness of the boundary layers on the upper and lower surfaces of the airfoil and the complete wake. This process is repeated until the maximum change in δ satisfies a specified convergence criterion.

Inviscid Solution Procedure

The integral appearing in Eq. (10) for the symmetric component of the pressure is approximated in the strong-interaction solution domain by the following second-order-accurate expression

$$\oint_{\bar{x}_{IB-1}}^{\bar{x}_{IE}} \frac{D_T'(\zeta)}{x_i-\zeta}\,d\zeta \approx \sum_{j=IB-1}^{IE-1} D_T'(x_{j+1})I_1(x_i;\bar{x}_j,\bar{x}_{j+1}) + \sum_{j=IB-1}^{IE-1} D_T''(x_{j+1})I_2(x_i;\bar{x}_j,\bar{x}_{j+1}) \tag{29}$$

where i and j are streamwise mesh point indices, IB and IE refer to the mesh stations at the beginning and end of the strong interaction solution domain, respectively, $\bar{x}_j=(x_{j+1}+x_j)/2$, and the functionals I_1 and I_2 are defined below. Although neglected here, contributions to the local (at $x=x_i$) pressure due to thickness effects from upstream ($0<\zeta<\bar{x}_{IB-1}$) and dowstream (at $\zeta>\bar{x}_{IE}$) of the strong interaction region can be determined by analytical or numerical integration (using trapezoidal rule quadrature) depending on the assumed functional form of the thickness distribution, $D_T(x)$. It is somewhat more difficult to determine the pressure difference component $[\![p_D^A]\!]$ because of the singular term $[\zeta/(1-\zeta)]^{1/2}$ which appears inside the integral on the right-hand side of Eq. (12). However, a first-order-accurate approximation to this integral has been determined and is given by

$$\oint_0^1 \frac{D_C'(\zeta)}{x_i-\zeta}\left(\frac{\zeta}{1-\zeta}\right)^{1/2} d\zeta \approx D_C'(0)I_3(x_i;0,\bar{x}_0) + D_C'(1)I_3(x_i;\bar{x}_{IT-1},1) + \sum_{j=0}^{IT-2} D_C'(x_{j+1})I_3(x_i;\bar{x}_j,\bar{x}_{j+1}) \tag{30}$$

where 0 and IT refer to the leading and trailing-edge mesh lines, respectively. The integral terms I_1, I_2, and I_3 appearing in Eqs. (29) and (30) are given by

$$I_n(x_i;\bar{x}_j,\bar{x}_{j+1})=\oint_{\bar{x}_j}^{\bar{x}_{j+1}} \frac{f_n(\zeta)}{x_i-\zeta}\,d\zeta, \quad n=1,2,3 \tag{31}$$

where $f_1=1$, $f_2=\zeta$, and $f_3=[\zeta/(1-\zeta)]^{1/2}$, and can be evaluated in closed form.

Once a converged solution to the strong displacement interaction problem is achieved, the inviscid pressure distribution must be corrected to account for wake curvature effects. The curvature of the reference wake streamline is determined by a numerical approximation to Eq. (14). Since $\kappa(x)$ must only be determined for $x>1$, the integral on the right-hand side of Eq. (14) can be evaluated by a simple trapezoidal rule quadrature. The pressure difference across the airfoil due to wake curvature effects $[\![p_{WC}^A]\!]$ is then determined by a numerical solution of the integral equation (13). This Fredholm integral equation of the first kind can be conveniently solved by first transforming the interval $[0,1]$ on the x axis to the interval $[0,\pi]$ on the unit circle and invoking certain properties of Chebyshev polynomials. The reader is referred to Ref. 1 for further details.

Viscous Solution Procedure

The viscous layer equations are solved numerically for a prescribed displacement thickness distribution. Solutions for the boundary layers on the upper and lower surfaces of the airfoil and for the complete wake are determined separately and by marching in the x direction. In each case the continuity and momentum equations are replaced by a set of linear algebraic equations using a finite difference approximation in which the nonlinear terms in the momentum equation for the $(n+1)$th iteration are linearized around the solution at the previous, (nth), iteration and the ξ and η derivatives are replaced by one-sided and central difference expressions, respectively. For the ξ derivatives, an upwind differencing scheme is used; i.e., backward differencing is used if $F>0$ and forward differencing is used if $F<0$. This results in a stable numerical algorithm in the presence of reverse flow and should be more accurate than the commonly used FLARE approximation[12] in which the streamwise convection terms are set to zero in reverse flow regions. The set of linear difference equations are then solved using a superposition technique. Essentially, the dependent variables F and V are decomposed into two components (e.g., $F=\beta F_I+F_{II}$) such that one component depends on the pressure gradient parameter β and the other component has no β dependence. As a result of this decomposition, two sets of linear algebraic equations are obtained. Final closure is achieved by determining the value of the pressure gradient parameter, using Eq. (25), such that the resulting solutions correspond to the prescribed value of displacement thickness.

In the authors' earlier studies[1,13] the viscous calculation procedure described previously was found to lead to satisfactory convergence rates for attached and mildly separated trailing-edge flows, when used in conjunction with the global viscous/inviscid iteration scheme of Eq. (28). However, in the present application to flows with relatively large reverse flow regions convergence difficulties were encountered. These are most pronounced near the separation and reattachment points, when the differencing direction for the $(n+1)$th viscous calculation is based on the previous [i.e., the (nth)] iterative solution. To overcome this problem an inner viscous iteration loop was incorporated into the global viscid/inviscid iteration. Thus the nonlinear terms in the momentum equation are updated at each streamwise station using intermediate $(n+1)$th-level viscous solutions. It was found that satisfactory convergence rates could be achieved for flows with large separation regions by simply performing the viscous iteration loop one time at each level of the global iteration scheme.

Results

The procedures outlined above have been applied to predict high Reynolds number laminar flow in the trailing-edge and near-wake regions of a thin airfoil. The airfoil geometry considered here has been selected to insure that the oncoming boundary layers remain attached until or shortly before the

trailing edge. Thus the symmetric part of the airfoil (i.e., the thickness distribution) is constructed from circular-arc trailing-edge sections which are smoothly joined to flat sections which extend to the leading edge. For the present purpose of analyzing local strong-interaction effects at the trailing edge there is no need to prescribe a closure at the leading edge of the airfoil. The antisymmetric part of the airfoil (i.e., the "camber" distribution) is determined from a prescribed pressure jump across the airfoil

Thus the airfoil surfaces are located at

$$y_{\pm}(x) = h_{\pm}(x) = \pm D_{T,A}(x) + D_{C,A}(x), \qquad x \in [0,1] \tag{32}$$

where $2D_{T,A}$ is the airfoil thickness and $D_{C,A}$ defines the location of the airfoil camberline. Here $D_{T,A}$ is given by

$$\begin{aligned} D_{T,A}(x) &= T/2, && 0 \le x \le x_c \\ &= T/2 - R + \sqrt{R^2 - (x - x_c)^2}, && x_c \le x \le 1 \\ &= 0, && x > 1 \end{aligned} \tag{33}$$

where T is the thickness of the airfoil, R the radius of curvature of the circular-arc trailing-edge section, i.e.,

$$R = [(T/2)^2 + (1 - x_c)^2]/T \tag{34}$$

and x_c is the point at which these circular-arc sections are joined to the flat sections of the symmetric airfoil. Following Veldman,[7] the inviscid pressure jump across the airfoil, $[\![p_A^A(x)]\!]$, is assumed to be constant upstream of the point $x = x_c$ and equal to that acting on a flat plate inclined at an angle α relative to the uniform stream for $x \le x_c \le 1$. Thus,

$$\begin{aligned} [\![p_A^A(x)]\!] &= \frac{-2\alpha}{(1 - M_\infty^2)^{1/2}} \frac{(1 - x_c)^{1/2}}{x_c^{1/2}}, && 0 < x < x_c \\ &= \frac{-2\alpha}{(1 - M_\infty^2)^{1/2}} \frac{(1 - x)^{1/2}}{x^{1/2}}, && x_c \le x \le 1 \\ &= 0, && x > 1 \end{aligned} \tag{35}$$

The foregoing pressure jump distribution corresponds to a thin cambered airfoil which more closely represents an inclined flat plate as $x \to 1$. The location of the airfoil camberline can be determined by numerical integration after setting $[\![p^A]\!] = [\![p_A^A]\!]$, $\kappa = 0$, and $D_C = D_{C,A}$ in Eq. (11) and $D_{C,A}(1) = 0$.

Numerical results will be presented for symmetric ($\alpha = 0$) and asymmetric, low-speed ($M_\infty = 0.1$), laminar flows at $Re = 10^6$ to illustrate the effects of airfoil thickness and loading on trailing-edge flow behavior and separation phenomena. However, it should be noted that the present analysis is also appropriate for high-speed, subsonic flow (c.f., Ref. 1). For the present calculations the value of x_c was set at 0.75. Further, viscous effects on the pressures in the trailing-edge region from upstream ($x < x_I = 0.5$) and downstream ($x > x_F = 1.5$) of the strong-interaction solution domain have been regarded as negligible. The extent of the viscous solution domain normal to the airfoil and wake streamline has been taken to be $7\delta_{BL}$ where δ_{BL} is the displacement thickness of the Blasius boundary layer. A total of 81 variably spaced mesh lines were used in the streamwise direction with a minimum spacing, $\Delta x_{min} \sim \mathcal{O}(\delta)$, of 0.003687 at the trailing edge. For the viscous calculation a uniform spacing in the normal direction was applied with a total of 41 points used for the upper- and lower-surface boundary-layer calculations and 81 points used for the wake calculation. Inviscid and viscous solutions were repeatedly determined for prescribed displacement thickness distributions until the maximum difference between the $(n+1)$th and nth diplacement thickness distribution over the strong-interaction solution interval was within 10^{-6}. The corresponding maximum difference between the viscous and inviscid pressures was approximately 5×10^{-4}. This level of convergence required less than 15 iterations using $\omega = 1$ in Eq. (28) for the attached flow solutions but as many as 150 iterations using underrelaxation with $\omega = 0.5$ for the most severe separated flow cases.

Symmetric Trailing-Edge Flow

Results indicating the effect of airfoil thickness on the flow in the trailing-edge region are shown in Fig. 2. Values of T equal to 0 (flat-plate airfoil), 0.005, 0.01, 0.015, and 0.02 are considered. For a double-circular-arc trailing-edge profile ($T > 0$), the viscous displacement thickness (Fig. 2a) increases very rapidly up to the trailing-edge point, thus smoothing the effective shape of the airfoil, and then drops very rapidly along the wake to an asymptotic value. The large growth in displacement thickness upstream of the trailing edge for $T > 0.01$ suggests the occurrence of flow separation. This is clearly indicated by the skin-friction coefficient C_f, and wake centerline velocity, u_{w}, distributions shown in Fig. 2b where negative values of C_f and u_{w} indicate reverse flow in the viscous layer. Note that the skin friction increases with increasing distance along the airfoil chord up to the trailing-edge point for the flat-plate airfoil but it decreases with increasing x for the double-circular-arc trailing-edge profiles. For $T \le 0.01$ the flow remains attached, but flow separation occurs for the 1.5% and 2.0%-thick airfoils. The streamwise extent of the reverse flow region for $T = 0.02$ is approximately 20% of airfoil chord. The wake streamline velocity for the attached, symmetric flows increases rapidly with distance from the trailing edge, while for the separated flows ($T = 0.015$ and 0.02) it increases with increasing distance from slightly upstream of the reattachment points which occur in the near wake.

First-order pressure (p) distributions are shown in Fig. 2c. Again the results for the flat-plate airfoil differ qualitatively from those for the thick airfoil. For the flat plate the pressure decreases up to the trailing-edge point and then rapidly increases with increasing streamwise distance to the freestream value ($p_\infty = 0$) in the near wake. For the double-circular-arc trailing-edge profiles the pressure generally increases with x up to the trailing edge and into the near wake, and then it gradually drops to its freestream value. Exceptions to this behavior occur for the 1.5%- and 2%-thick airfoils, but particularly for the latter, where pressure plateaus, typical of separated flow, form in the immediate vicinity of the trailing edge.

The differences in flow behavior for the flat plate and the thick airfoils can be explained as follows. The sudden removal of the no-slip condition at the trailing edge causes the flow to accelerate in the streamwise direction resulting in a thinning of the boundary layer, an increase in skin friction and a decrease in pressure as the trailing edge is approached. This behavior is reflected by the flat-plate results shown in Fig. 2. However, thick-airfoil closure (in a finite trailing-edge angle) causes the flow to decelerate as it approaches the trailing-edge point leading to a thickening of the boundary layer along with a decrease in skin friction and increase in pressure. The results depicted in Fig. 2 reveal that even for a very small thickness ($T = 0.005$) the decelerating effect due to airfoil closure is stronger than the accelerating effect due to the relief of the no-slip condition.

Asymmetric Trailing-Edge Flow

Results indicating the effect of loading on the flow in the vicinity of the trailing edge of a 1%-thick airfoil are shown in Fig. 3. Values of α [c.f., Eq. (35)] equal to 0 (symmetric flow), 0.035 and 0.07 are considered. Similar results for a zero-thickness ($T = 0$) airfoil have been reported previously in Ref. 1. Suction surface boundary-layer and wake displace-

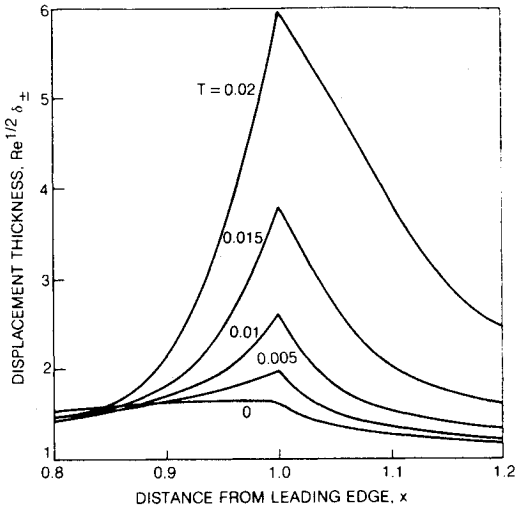

a) Displacement thickness distributions.

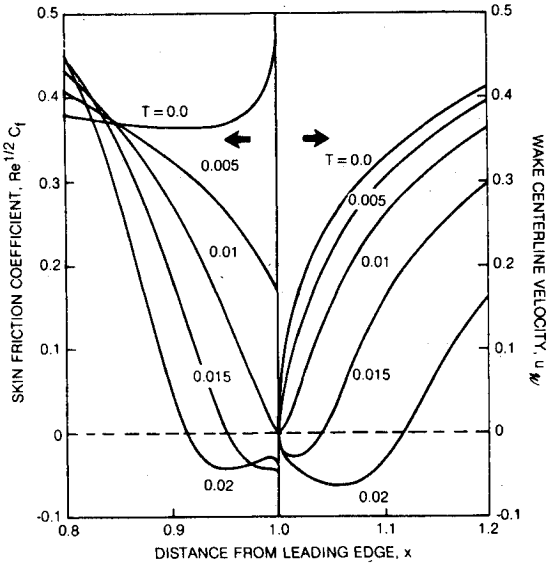

b) Skin friction and wake centerline velocity distributions.

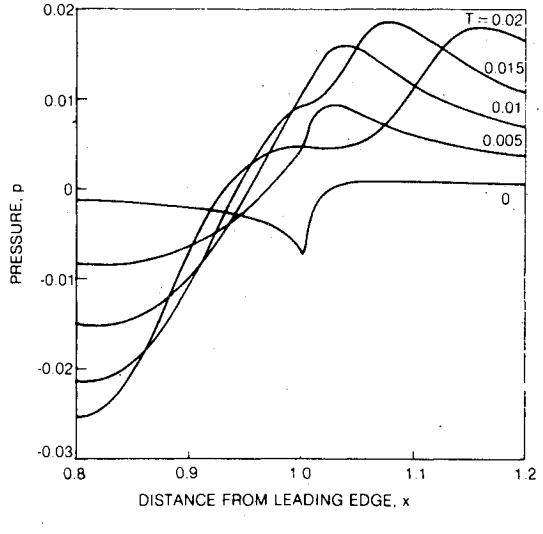

c) Pressure distributions.

Fig. 2 Symmetric trailing-edge flow: effect of thickness. $M_\infty = 0.1$; $Re = 10^6$; $\alpha = 0$.

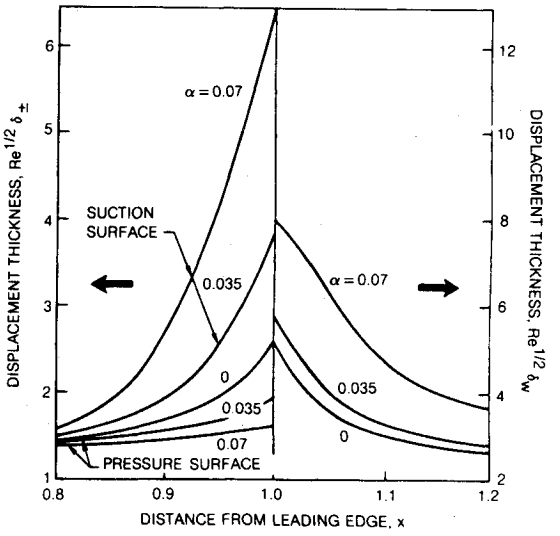

a) Displacement thickness distributions.

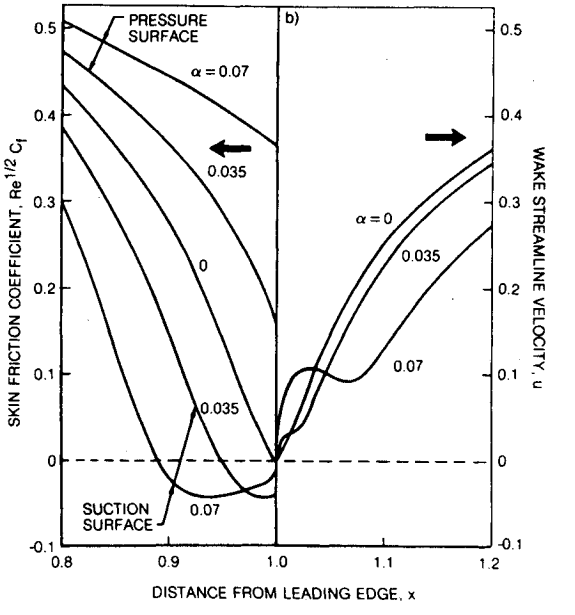

b) Skin friction and wake streamline velocity distributions.

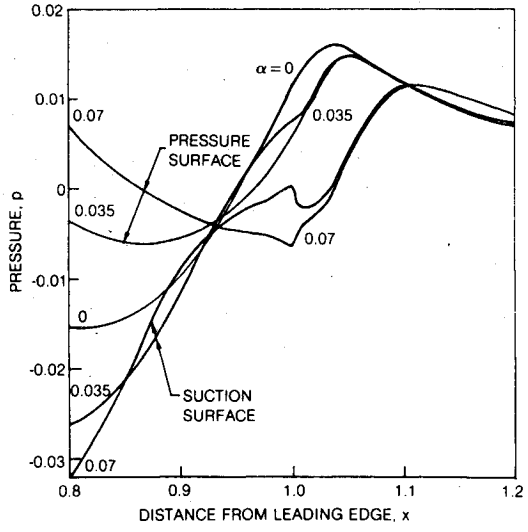

c) Pressure distributions.

Fig. 3 Asymmetric trailing-edge flow: effect of loading. $M_\infty = 0.1$; $Re = 10^6$; $T = 0.01$.

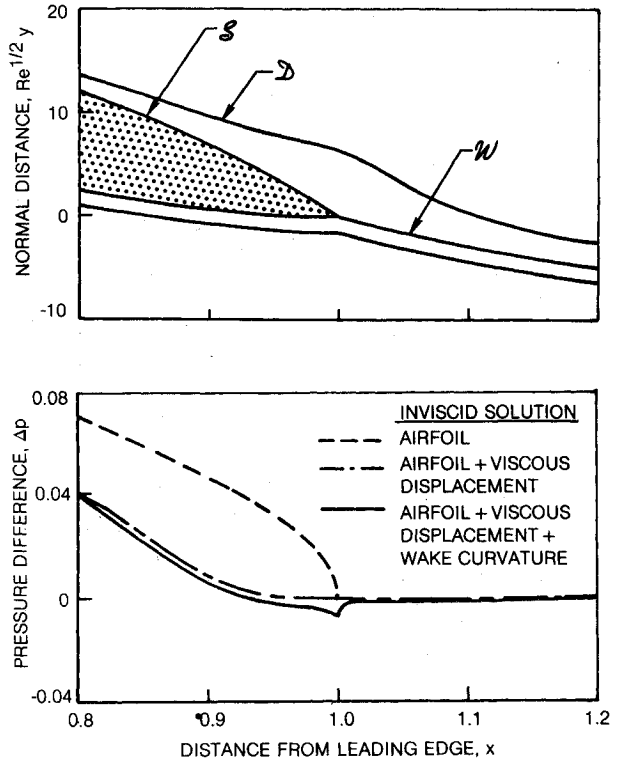

Fig. 4 Viscous effects in the trailing-edge region of a 1%-thick, loaded airfoil. $M_\infty = 0.1$; $Re = 10^6$; $T = 0.01$; $\alpha = 0.07$.

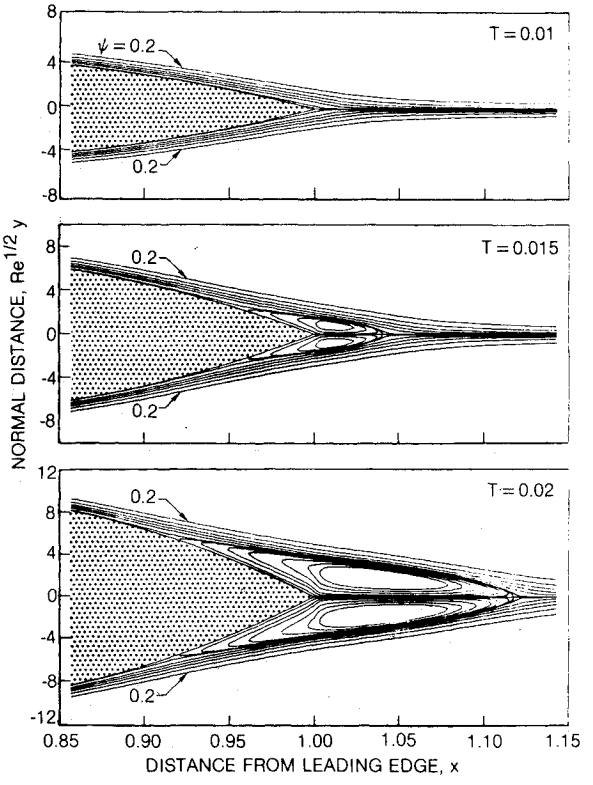

Fig. 5 Effect of thickness on trailing-edge streamline pattern for symmetric flow with $M_\infty = 0.1$, $Re = 10^6$, and $\alpha = 0$.

ment thicknesses (Fig. 3a) increase dramatically with an increase in airfoil loading, but there is a thinning of the pressure surface boundary layer with increasing α. The skin-friction distributions shown in Fig. 3b indicate that for a 1%-thick airfoil the flow separates from the suction surface at approximately $x = 0.94$ for $\alpha = 0.035$ and at $x = 0.89$ for $\alpha = 0.07$. The existence of reverse flow in the wake is not obvious from the wake streamline velocity distributions depicted in Fig. 3b, since the reference wake streamline lies below the separation bubbles which occur at $\alpha = 0.035$ and 0.07, and hence, $u_w > 0$. However, the leveling off of the wake streamline velocity just aft of the trailing edge signals that the flow has separated from the suction surface of the airfoil. The pressure distributions for the 1%-thick airfoils are shown in Fig. 3c. Note that for $\alpha = 0.07$ there is a strong adverse pressure gradient on the suction surface which is associated with the existence of a relatively large separation bubble and a correspondingly thick suction surface boundary layer.

Although the contribution to the lift acting on the airfoil from the loading in the trailing-edge region (i.e., $x > 0.8$) increases with increasing α (Fig. 3c), viscous effects cause a significant reduction in the lift that would be predicted from inviscid considerations alone. In general, both displacement and wake curvature effects tend to decrease the loading on the airfoil, but at a Reynolds number of 10^6 the effect of wake curvature is generally much smaller than that of viscous displacement. The viscous influence on the effective shape and on the loading or pressure difference (i.e., $\Delta p = -[\![p]\!]$) distribution for the 1%-thick airfoil with $\alpha = 0.07$ is illustrated in Fig. 4. Here the pressure difference distributions due to 1) the airfoil alone, 2) the airfoil and viscous displacement effects, and 3) the airfoil, viscous displacement, and wake curvature effects are depicted. Flow separation gives rise to a relatively thick suction-surface boundary layer. Thus displacement effects tend to "uncamber" the airfoil leading to a substantial reduction in the loading over the trailing-edge region. Wake curvature effects further reduce the loading and give rise to a negative loading in the immediate vicinity of the trailing edge.

A comparison of the results for the 1%-thick airfoils (Fig. 3) with those for zero-thickness airfoils (Fig. 3 of Ref. 1) reveals that airfoil thickness has a significant impact on the behavior of the flow in the vicinity of a loaded trailing edge. In particular, an increase in airfoil thickness greatly enhances the likelihood of flow separation from the suction surface of the airfoil, and it produces a substantially thicker suction-surface boundary layer. In addition, less favorable pressure gradients and smaller shear stresses occur on the pressure surface of the airfoil.

Trailing-Edge Streamline Patterns

It is instructive to examine the flow in the trailing-edge region via streamline contours. Values of the stream function in the viscous layer, $\psi(x,\bar{y})$, are determined from the relation

$$\psi = \int_0^{\bar{y}} \rho u \, d\bar{y} = \sqrt{2\xi} \int_0^{\eta} F \, d\eta \tag{36}$$

where ψ is taken to be zero on the surfaces of the airfoil and on the reference wake streamline; i.e., at $\bar{y} = 0$. After evaluating ψ at the mesh points used in the viscous-layer calculation a standard contour plotting package has been applied to map lines of constant ψ and to produce the streamline plots shown in Figs. 5 and 6.

Trailing-edge streamline patterns for the 1, 1.5, and 2%-thick symmetric airfoils are shown in Fig. 5. For the 1%-thick case the flow remains attached to the airfoil surfaces. However, a small reverse flow region, which extends over approximately 8% of chord, occurs for the flow around the 1.5%-thick airfoil, and a much larger region of reverse flow, which extends over approximately 20% of chord, occurs for the 2% thick airfoil. The streamline contours indicate that the reverse flow region consists of a pair of counter-rotating eddies. These eddies cause that part of the flow which moves in the streamwise direction to lift off the airfoil surface and reattach in the near wake on the line of symmetry; i.e., on the x axis or wake centerline.

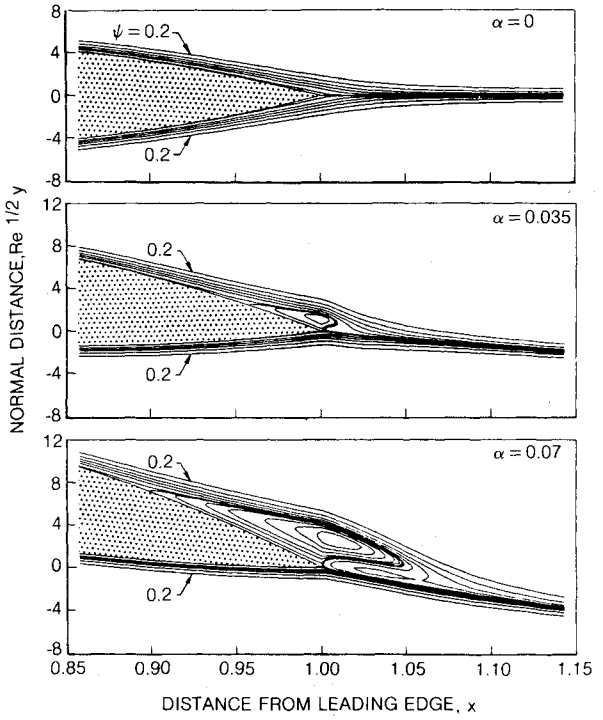

Fig. 6 Effect of loading on trailing-edge streamline pattern for asymmetric flow with $M_\infty = 0.1$, $Re = 10^6$, and $T = 0.01$.

Asymmetric trailing-edge streamlines are shown in Fig. 6. Flows past 1%-thick airfoils with values of $\alpha = 0$ (symmetric flow, no loading), 0.035 and 0.07 are depicted. For the $\alpha = 0$ case (also shown in Fig. 5) the flow remains attached to the airfoil surfaces, but separation occurs on the suction surface of the 1%-thick airfoil even at a very small value of the loading parameter (i.e., $\alpha = 0.035$) with the extent of the reverse flow region increasing with increasing α. For $\alpha = 0.035$ (Fig. 6) the flow separates from the suction surface of the airfoil at $x = 0.94$ and for $\alpha = 0.07$ it separates at $x = 0.89$. In both cases it reattaches at the trailing edge.

There are remarkable differences between the separated flow patterns for the symmetric and asymmetric airfoils. For symmetric flows the flow separates from both surfaces of the airfoil and rattaches in the wake, and the reverse flow region is made up of a pair of counter-rotating eddies. In the asymmetric case, a one-sided separation occurs in which the flow separates from the suction surface and reattaches at the trailing edge. Further, the reverse flow region adjacent to the suction (upper) surface consists of a single eddy in which the flow moves in the clockwise (for $\alpha > 0$) direction. For the large bubble at $\alpha = 0.07$ (Fig. 6) the dividing streamline extends well into the wake before turning back and impinging on the airfoil surface. In addition, a subtle feature displayed by the streamline pattern for the large asymmetric separation bubble is the existence of a secondary reverse flow region which lies downstream of the trailing edge and above the reference wake streamline. Both the primary and secondary reverse flow eddies cause the wake streamline velocity u to remain relatively constant over a segment of the near-wake streamline (c.f., Fig. 3b) before it accelerates to its freestream value.

The computational grid used for the foregoing calculations was not fine enough to uncover the small region of highly favorable pressure gradient in the immediate vicinity of the trailing edge identified by Smith.[5] It is this gradient which causes the flow to reattach just upstream of the trailing edge leading to forward flow on both the suction and pressure surfaces of the airfoil at the trailing-edge point, as required by the Rott-Hakkinen condition.[2] In the present calculation of asymmetric trailing-edge separation, the flow is forward at the first mesh point on the reference wake streamline off the trailing edge, but there is no indication of reattachment just upstream of the trailing edge. However, within reasonable limits the present solutions demonstrate that a one-sided separation with the reverse flow region abruptly closing at the trailing edge can be predicted with a finite Reynolds number interaction analysis.

Concluding Remarks

An analytical procedure based on finite Reynolds number viscous/inviscid interaction theory has been developed to predict subsonic flow in the trailing-edge and near-wake regions of an airfoil, and numerical results have been presented for symmetric and asymmetric laminar flows past a prescribed family of airfoil trailing edges. Using the analytical and numerical methods described herein, converged viscous/inviscid interaction solutions have been achieved for trailing-edge flow separations extending up to 20% of airfoil chord. The important consequence of the present study is the demonstration that local separation phenomena in the vicinity of an airfoil trailing edge, including one-sided separations for loaded airfoils, can be predicted using a finite Reynolds number viscous/inviscid interaction model.

In particular, relatively large reverse flow regions have been determined for symmetric flow around a 2%-thick double-circular-arc trailing edge and for asymmetric flow around a trailing edge defined by a 1%-thick double-circular-arc thickness distribution and a camber distribution determined by setting the loading parameter (or trailing-edge angle of attack) α in Eq. (35) equal to 0.07. In the symmetric case the reverse flow region consists of a pair of counter-rotating eddies with the streamlines separating the regions of forward and reverse flow lifting off the upper and lower surfaces of the airfoil upstream of the trailing edge and reattaching in the near wake on the wake centerline. For the asymmetric case, the primary reverse flow region lies adjacent to the suction surface of the airfoil and consists of a single eddy in which the fluid moves in the clockwise (for $\alpha > 0$) direction. Here the dividing streamline departs from the airfoil suction surface and subsequently reattaches on this surface just before merging into the wake. In addition, there is a small secondary reverse flow region in the near wake which lies above the reference wake streamline. It should be noted that the separation patterns determined here using the finite Reynolds number, interacting-boundary-layer model are in qualitative agreement with those predicted using the asymptotic ($Re \to \infty$) triple-deck equations,[5,6] and with the experimental observations (for turbulent flows) of Refs. 14 and 15.

Acknowledgment

This research was sponsored by the Naval Air Systems Command under Contract N62271-82-M-2797. The assistance provided by Dr. R. P. Shreeve, NASC Program Manager for this contract, is gratefully acknowledged.

References

[1]Vatsa, V. N. and Verdon, J. M., "Viscous/Inviscid Interaction Analysis of Asymmetric Trailing-Edge Flows," *Numerical and Physical Aspects of Aerodynamic Flows II*, edited by T. Cebeci, Springer Verlag, New York, 1984, pp. 205-221.

[2]Rott, N. and Hakkinen, R. J., "Similar Solutions for Merging Shear Flows," *Journal of the Aerospace Sciences*, Vol. 29, Sept. 1962, pp. 1134-1135.

[3]Brown, S. N. and Stewartson, K., "Trailing-Edge Stall," *Journal of Fluid Mechanics*, Vol. 42, Pt. 3, 1970, pp. 561-584.

[4]Chow, R. and Melnik, R. E., "Numerical Solutions of the Triple Deck Equations for Laminar Trailing-Edge Stall," *Proceedings of 5th International Conference on Fluid Dynamics, Lecture Notes in Physics*, Vol. 59, 1976, pp. 135-144.

[5]Smith, F. T., "Interacting Flow Theory and Trailing-Edge Separation-No stall," *Journal of Fluid Mechanics*, Vol. 131, June 1983, pp. 219-250.

[6]Smith, F. T., "On the High Reynolds Number Theory of Laminar Flows," *IMA Journal of Applied Mathematics*, Vol. 28, May 1982, pp. 207-281.

[7]Veldman, A. E. P., "The Calculation of Incompressible Boundary Layers with Strong Viscous-Inviscid Interaction," *AGARD Symposium on Computation of Viscous-Inviscid Flows*, AGARD-CPP-291, 1980, Chap. 12.

[8]Veldman, A. E. P., "New Quasisimultaneous Method to Calculate Interacting Boundary Layers," *AIAA Journal*, Vol. 19, Jan. 1981, pp. 79-85.

[9]Brown, S. N. and Stewartson, K., "Wake Curvature and the Kutta Condition in Laminar Flow," *The Aeronautical Quarterly*, Vol. 26, 1975, pp. 275-280.

[10]Ashley, H. and Landahl, M., *Aerodynamics of Wings and Bodies*, Addison Wesley Publishing Co., Reading, Mass., 1965, pp. 88-97.

[11]Carter, J. E., "A New Boundary Layer Interaction Technique for Separated Flows," AIAA Paper 79-1450, Williamsburg, Va., July 1979.

[12]Reyhner, T. A. and Flügge-Lotz, I., "The Interaction of a Shock Wave with a Laminar Boundary Layer," *International Journal on Nonlinear Mechanics*, Vol. 3, No. 2, 1968, pp. 173-179.

[13]Vatsa, V. N., Werle, M. J., and Verdon, J. M., "Viscid/Inviscid Interaction at Laminar and Turbulent Symmetric Trailing Edges," AIAA Paper 82-0165, Orlando, Fla., Jan. 1982.

[14]Nakayama, A., "Measurements of Attached and Separated Flows in the Trailing-Edge Regions of Airfoils," *Numerical and Physical Aspects of Aerodynamic Flows II*, edited by T. Cebeci, Springer Verlag, New York, 1984, pp. 233-255.

[15]Adair, D., Thompson, B. E., and Whitelaw, J. H., "Measurements and Calculations of a Separating Boundary-Layer and the Downstream Wake," *Numerical and Physical Aspects of Aerodynamic Flows II*, edited by T. Cebeci, Springer Verlag, New York, 1984, pp. 97-112.